JOURNAL OF SPACECRAFT AND ROCKETS
Vol. 46, No. 3, May–June 2009

Engineering Notes

ENGINEERING NOTES are short manuscripts describing new developments or important results of a preliminary nature. These Notes should not exceed 2500 words (where a figure or table counts as 200 words). Following informal review by the Editors, they may be published within a few months of the date of receipt. Style requirements are the same as for regular contributions (see inside back cover).

Photometric Detection of Known Sun-Occluding Satellites

Brian J. Poller* and Robert D. Culp†
University of Colorado, Boulder, Colorado 80309

DOI: 10.2514/1.41593

I. Introduction

A DAY-TIME method of detecting satellites by observing the occlusion of direct sunlight in discrete digital images is suggested. This method of detection, which also measures the total occluding area of a satellite's shadow, is tested empirically for observations of the Terra EOS-AM1 (Earth Observation System: Morning Platform) satellite.

Previously, in [1,2], a matched filter detection method was developed for optical observations of sunlight-reflecting satellites and orbital debris, which appear as faint streaks in the pixels of stellar background images and cause photometric signal changes independent of the pixel background signals. This matched filter detection method calls, first, for a set of timed sequential images to be normalized as a three-dimensional data set and, second, for discrete spatial temporal paths through the data set to be summed as detection tests. The coordinates required to define each pixel location are the discrete spatial pixel coordinates $\{i, j\}$, where $\{i = 1, \ldots, L, j = 1, \ldots, M\}$, and the temporal frame number $\{k\}$, where $\{k = 1, \ldots, N\}$. In the normalization step, a pixel location with instantaneous signal value S_{ijk} is replaced by some calculated or normalized value termed d_{ijk}.

In this Note, an alternative method of optically observing satellites and orbital debris is developed. The proposed observation occurs during the day when an object crosses between the sun and an observer, occluding direct sunlight and creating an object shadow. These observations take the form of discrete digital images, and a matched filter detection method is applied. As with other matched filter applications, this detection method is only effective for known objects, or objects predicted to transit the sun with a known motion and bearing. The motion and bearing parameters dictate a spatial temporal filter designed to integrate the occluded pixel locations along an object's transit path.

II. Detection of Occluded Sunlight over Pixels in a Matched Spatial Temporal Path

The photometric signal change due to an occluding shadow has been previously developed and used for the detection of star-occluding extra-solar planets. By measuring periodic changes in the signal level of the total light of a star due to a planetary occlusion, the size of an extra-solar planet can be determined with respect to the size of its parent star. This photometric measurement of planet size with respect to star size has been termed transit depth [3]. The calculation of transit depth should be compared to the linear pixel normalization technique developed for matched filter detection in [2]. Assuming Poisson statistics, the form of the linear normalization technique in [2] is, in fact, equivalent to the calculation of transit depth in [3] for a discrete, $\{i, j, k\}$ pixel location by a change of sign. Here, changing the sign of the linear normalization defines a pixel occlusion ratio which is formed as d_{ijk} at each and every pixel location in a data set. This pixel occlusion ratio is calculated as follows:

$$d_{ijk} = \frac{\bar{S}_{ij} - S_{ijk}}{\bar{S}_{ij}} = \frac{\text{area}_{\text{occlusion}}ijk}{\text{area}_{\text{pixel}}} \tag{1}$$

If some $\{i, j, k\}$ pixel location contains an occluding shadow, then the normalized value d_{ijk} represents the area of that occlusion encompassed in that pixel location, termed $\text{area}_{\text{occlusion}}ijk$. Consistent with the determination of transit depth, this occluding area is scaled to the discrete area of one pixel, termed $\text{area}_{\text{pixel}}$. In Eq. (1), $\bar{S}_{ij}$ represents the background signal of the $\{i, j\}$ pixel when it is not being occluded. If it is not known in advance, $\bar{S}_{ij}$ can be calculated, from [1], as the temporal mean of the $\{i, j\}$ pixel location over the time of N considered frames as follows:

$$\bar{S}_{ij} = \frac{1}{N}\sum_{k=1}^{N} S_{ijk} \tag{2}$$

It is useful to define $\Delta S_{ijk} = \bar{S}_{ij} - S_{ijk}$ as the expected instantaneous signal change due to an occluding shadow at pixel location $\{i, j, k\}$. Then Eq. (1) can be rewritten as follows:

$$\Delta S_{ijk} = \frac{\text{area}_{\text{occlusion}}ijk}{\text{area}_{\text{pixel}}} \cdot \bar{S}_{ij} \tag{3}$$

As shown in Eq. (3), this expected instantaneous signal change ΔS_{ijk} is dependant upon two factors: the size of the occluding shadow relative to the size of a pixel, and the signal level of the sun background $\bar{S}_{ij}$ in the $\{i, j\}$ pixel location being occluded.

Now, we wish to consider integrating paths of pixel occlusion ratios d_{ijk} from Eq. (1). These spatial temporal paths are formed from a series of square spatial neighborhoods. For example, Fig. 1 shows a $m \times m$ pixel neighborhood, centered at a spatial $\{i, j\}$ pixel location at frame $\{k\}$.

If a neighborhood of normalized pixel locations completely contains an occluding shadow, then the sum of the neighborhood gives the total occluding area of the shadow at frame $\{k\}$. This total occluding area will be in units of pixel areas because each pixel occlusion ratio is scaled to one pixel area by Eq. (1). Pixel locations, normalized as d_{ijk}, but not containing an occluding shadow, will have an expected value of zero So, if the considered neighborhood is larger than the total occluding area, the summation of a neighborhood should still report the total occluding area of an observed satellite shadow, as long as it is completely contained in that neighborhood.

Received 29 October 2008; revision received 14 February 2009; accepted for publication 14 February 2009.

*Graduate Student, Department of Aerospace Engineering Sciences.
†Professor, Department of Aerospace Engineering Sciences, Colorado Center for Astrodynamics Research. Fellow AIAA.

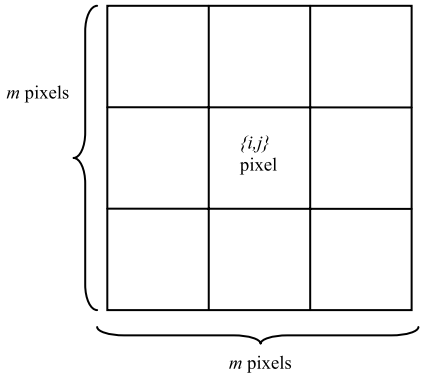

Fig. 1 Example of $m \times m$ neighborhood at frame $\{k\}$

Because the considered paths are made of a series of m pixel by m pixel square neighborhoods in each of n sequential frames, the total path contains nm^2 pixel locations. A matched filter detection test is made by summing such a path. If the considered spatial temporal path is, indeed, matched to the observed motion of the occluding object, then the value of this detection test will be the total occluding area of the shadow multiplied by n, the number of frames in the transit.

III. Experimental Measurement of Satellite-Occluding Area

An experimental test was performed with the purpose of detecting sunlight-occluding satellites and rocket bodies, and measuring the total occluding area of those objects over predicted spatial temporal paths. Optical observations were recorded with a Meade telescope with 90-mm-diam aperture and a Lumenera monochrome camera, recording 12-bit, 640×480 pixel images at 60 frames per second. An optically dense Thousand Oaks solar filter was required to prevent sunlight from saturating the detector array, and a Mogg focal reducer was required to fit four corners of the sun's perimeter in the detector image.

The only object repeatedly detected was the Terra EOS-AM1 satellite, which was observed in transit on July 2007 and July 2008. This satellite's occluding shadow became distinctly visible moving north to south through sequential images which were normalized by forming a temporal mean frame and replacing all pixel locations with pixel occlusion ratios in accordance with Eq. (1). Figure 2a depicts the 2007 transit event by projecting sections of the 36 total frames, containing the satellite's occluding shadow, along the transit path. The 2008 north-to-south transit event is depicted in Fig. 2b by projected sections of the 43 frames along that transit path.

During the transits, the satellite had ranges of 780 and 783 km from the observer (in 2007, 2008). Both events had a similar geometry of detection formed between the positions of the observer, the satellite, and the sun because they were observed from the same location at similar times, a year apart: 12 July 2007 16:40:41 UTC and 14 July 2008 16:40:31 UTC. However, in the 2007 transit (Fig. 2a), the telescope imaged from an indoor location through the solar filter and an additional glass window, unlike 2008 (Fig. 2b) when the telescope was outside, imaging the sun directly through the solar filter. The drawn compasses are only approximations. To convey the correct orientation of the image plane in that patch of sky, they should actually be rotated by the parallactic angle, which depends on the pointing direction of the equatorially mounted telescope.

The two transit images are rotated by several degrees from each other and neither would match the compass directions precisely because of polar misalignment and rotation of the camera in the telescope eyepiece. One detractor in making accurate orbital measurements with these observations is that image alignment cannot be generally determined from the image itself, and so it requires experimental knowledge of the rotation of the sun image on the detector array.

The Terra satellite, recorded in the transits, is known to possess a large solar array area of 45 m^2 rotating on one axis to always face the sun [4]. Given the 582.7-mm focal length of the experimental system, each square image pixel subtends 7.2×10^{-4} deg along the edge. At the range of the satellite, the total occluding area of the satellite shadow is predicted to be 0.5 ± 0.05 pixel areas. Because of the difficulty of precisely determining the orientation and area of the satellite bus, an error of 0.05 pixel areas is assumed.

For the two transits events, matched spatial temporal paths were formed from $m \times m$ pixel neighborhoods, each containing the Terra satellite shadow. In Figs. 3a and 3b the total occluding area of the Terra satellite is plotted as an accumulated mean of the total occluding area of neighborhoods per the number of sequential frames considered for each 2007 and 2008 event. Plots of the total occluding area of the satellite are trended over increasing values of m, denoting larger $m \times m$ pixel neighborhoods containing the occlusion. In comparison to these occluded paths, Fig. 3c shows the total occluding area, as calculated, over neighborhoods of pixel occlusion ratios where the satellite's occluding shadow is absent

In Figs. 3a and 3b, as the $m \times m$ neighborhood size increases, the calculated total occluding area of those neighborhoods converges to the predicted value for the Terra satellite of 0.5 ± 0.05 pixel areas. The reason why the $m = 3, 5$, and 7 neighborhoods do not report the full predicted value is because the occluded shadow is blurred over areas larger than those neighborhood sizes. An increased blurring occurred in the 2007 transit due to additional window glass, causing the neighborhood sizes of $m = 3, 5$, and 7 in Fig. 3b to report smaller total occluding areas than in the same neighborhoods in Fig. 3a. As the neighborhood size increases, a larger spatial path is integrated, and this compensates for the spatial blurring but at a cost of reduced resolution.

There may be some ways to reduce this optical blurring experimentally. Because of telescope diffraction and atmospheric turbulence, a circular blurring as a point spread function with a maximum diameter of 4 pixels was expected, but the extent of spatial diffusion of the shadow in Figs. 2a and 2b exhibits a point spread function diameter of over 7 pixels. This level of blurring may be due to chromatic aberration, which occurs when light of different wavelengths refracts through a material (like a prism). The experimental system had several layers of refracting glass including the solar filter, telescope aperture, focal reducer, and the glass window in

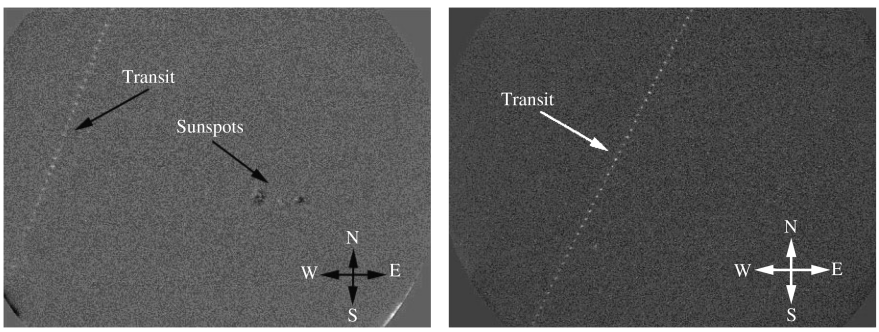

a) b)

Fig. 2 Terra transit on a) July 2007, and b) July 2008.

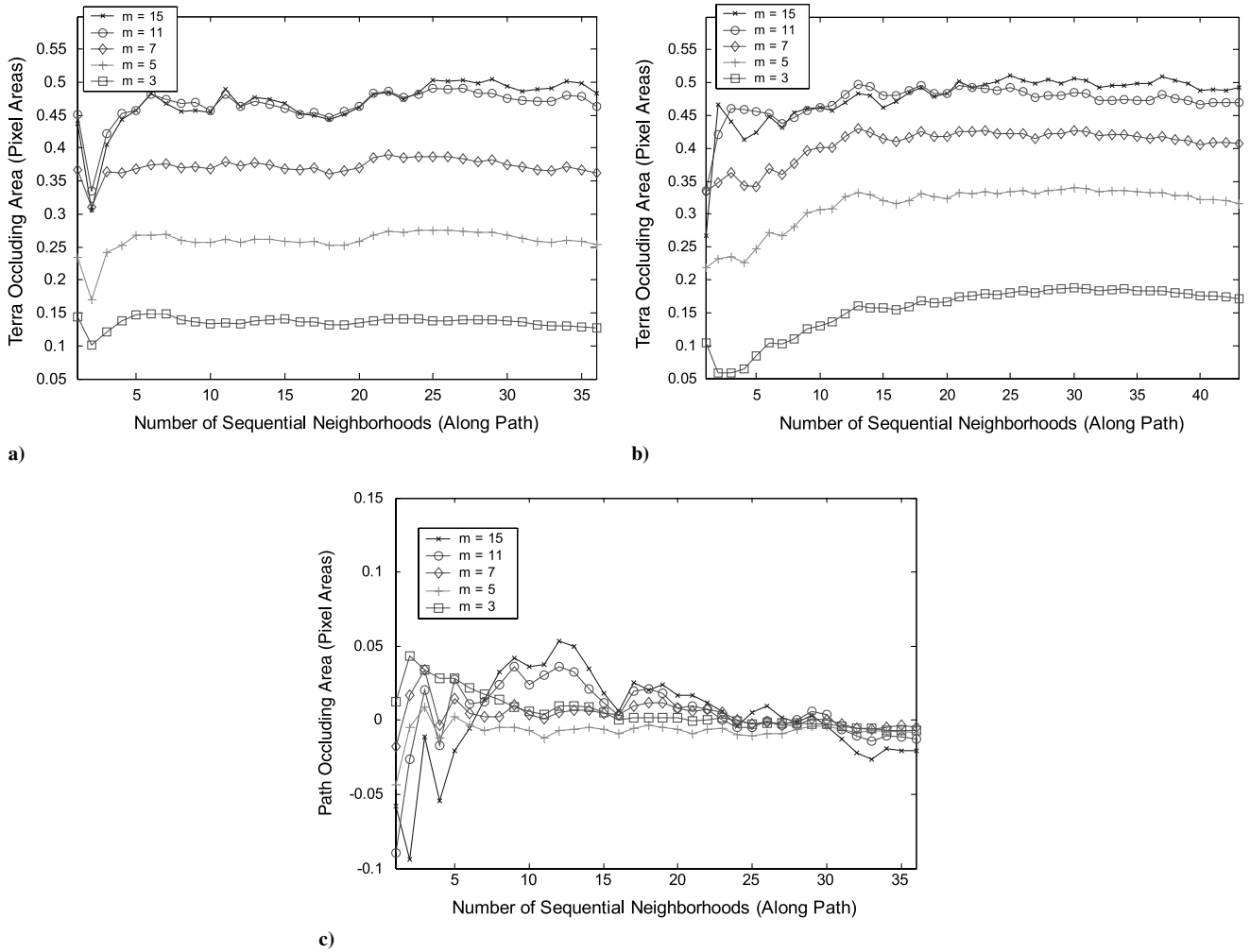

Fig. 3 Average occluding area in $m \times m$ neighborhoods containing a) 2007 Terra shadow, b) 2008 Terra shadow, and c) no shadow.

the 2007 transit. Because the sun was observed in white light (over a continuum of wavelengths), it is likely that chromatic aberration could cause a circular blurring in the image with a diameter greater than 7 pixels. A test for this hypothesis would require making a set of transit observations using a narrower bandpass filter, instead of a white light continuum filter.

The initial dips in Figs. 3a and 3b occurring in the first five frames show variations in the total occluding area of the satellite shadow. A number of factors can scatter light into the shadowed region and reduce the depth of the shadow. Scattering of light in the telescope should result in very small intensity changes over time. Scattering of light in the atmosphere due to turbulence is likely to dominate the intensity fluctuations of the detected shadow. Instantaneously, scintillation causes random variations of intensity of the light reaching the detector, but, over frames, these instantaneous variations should be averaged out. From Eq. (1), as long as the total occluding area of a shadow is constant over a path, then the summed neighborhood of d_{ijk} should also be constant. Then background variations at each $\{i, j\}$ pixel location, for example, limb darkening, should not affect d_{ijk} over frames.

IV. Theoretical Resolution Limit of a Constant False Alarm Rate Detector

Of particular interest is the resolution of these spatial temporal paths in use for detection of smaller sun-occluding objects, especially as the total occluding area becomes much smaller than one pixel area. According to the central limit theorem [5], a z-score detection statistic can be measured (in standard deviations) by comparing the path summation, containing the occluding satellite, with the distribution of all other parallel path summations of equal length. If we consider a path as a sample of pixel occlusion ratios taken from the population of pixel occlusion ratios distributed with a mean value μ_d and standard deviation σ_d, then, dividing a path summation by the total number of pixel locations in that path forms a sample mean. In Sec. II, it was stated that the summation of a matched path over n frames, encompassing an occluding shadow, is equivalent to the value of the total occluding area multiplied by n. Then, if the total number of pixel locations in the path is nm^2, the sample mean of a matched path can be written as the total occluding area divided by m^2. Then, the z score of a matched path containing an occluding object can be expressed as follows:

$$z = \frac{\text{total}_{\text{occluding}}\text{area}/m^2 - \mu_d}{\sigma_d \sqrt{1/nm^2}} \tag{4}$$

In Eq. (4), the denominator is the standard error of the sample means, which is the population standard deviation multiplied by $\sqrt{1/nm^2}$. To derive population statistics μ_d and σ_d, it is useful to write the pixel occlusion ratios in terms of photon counts. From [6], a constant scale factor is used to convert the instantaneous and mean signal quantities S_{ijk} and $\bar{S}_{ij}$ into their respective instantaneous and mean photon quantities R_{ijk} and λ_{ij}. Applying this scale factor to the numerator and denominator terms of Eq. (1) gives another right-hand side to the pixel occlusion ratio:

$$d_{ijk} = \frac{\lambda_{ij} - R_{ijk}}{\lambda_{ij}} \tag{5}$$

In Eq. (5), λ_{ij} is the mean photon counts expected at the $\{i, j\}$ pixel location. This term is also a Poisson parameter, defining the mean

and variance of the distribution of instantaneous random variables R_{ijk} measured over N frames at a given $\{i, j\}$ pixel location. The number of statistically considered frames N can be arbitrarily greater or less than n, the number of frames recording a transit event. If λ_{ij} is the Poisson mean value of the distribution of R_{ijk} in each $\{i, j\}$ pixel location over N frames, the following identity can be written:

$$\frac{1}{N}\sum_{k=1}^{N}(\lambda_{ij} - R_{ijk}) = (0)_{ij} \tag{6}$$

A second identity can be written, because λ_{ij} is the Poisson variance of the distribution of R_{ijk} in each $\{i, j\}$ pixel location over N frames:

$$\frac{1}{N}\sum_{k=1}^{N}(\lambda_{ij} - R_{ijk})^2 = \lambda_{ij} \tag{7}$$

Now, we approximate μ_d and σ_d for the population of pixel occlusion ratios. First, for μ_d, the size of the population is considered to have spatial dimensions of L and M pixels, and N temporal frames:

$$\mu_d = \frac{1}{LMN}\sum_{i=1}^{L}\sum_{j=1}^{M}\sum_{k=1}^{N}\frac{\lambda_{ij} - R_{ijk}}{\lambda_{ij}} \tag{8}$$

Equation (8) can be simplified by applying Eq. (6), then μ_d, the mean of the population of pixel occlusion ratios, is seen to be zero:

$$\mu_d = 0 \tag{9}$$

Next, the calculation of the population standard deviation σ_d is formed as follows:

$$\sigma_d = \sqrt{\frac{1}{LMN}\sum_{i=1}^{L}\sum_{j=1}^{M}\sum_{k=1}^{N}\left(\frac{\lambda_{ij} - R_{ijk}}{\lambda_{ij}} - \mu_d\right)^2} \tag{10}$$

Equation (10) can be simplified by first applying Eq. (7):

$$\sigma_d = \sqrt{\frac{1}{LM}\sum_{i=1}^{L}\sum_{j=1}^{M}\frac{1}{\lambda_{ij}}} \tag{11}$$

Equation (11) is further simplified by assuming that the expected photon count in each pixel of the sun background is the same. This assumption provides a useful approximation, but ignores the spatial variations of the sun background, for example, sunspots and limb darkening. This approximation is made by defining λ as the spatial temporal mean of all pixel locations in the sun background. Then, setting $\lambda_{ij} = \lambda$ for all $\{i, j\}$ in Eq. (11) produces an approximate population standard deviation:

$$\sigma_d = \sqrt{\frac{1}{\lambda}} \tag{12}$$

In Eq. (12), λ is a unitless count. Inserting Eqs. (9) and (12) into Eq. (4) and simplifying approximates the z- detection statistic:

$$z = \text{total}_{\text{occluding}}\text{area}\sqrt{\frac{\lambda n}{m^2}} \tag{13}$$

Equation (13) approximates the maximum detection statistic, which can be attained from a matched spatial temporal path, consisting of $m \times m$ neighborhoods, each containing an occluding object, over n frames. This z-detection statistic is linearly proportional to the total occluding area of the satellite, assuming that this is constant over the n frames of the transit. The detection statistic is governed by the variance of the Poisson parameter λ, representing the approximated photon count in each sun background pixel. Also, the path parameters n and m affect the z-detection statistic. For instance, z can be increased by reducing the size of the $m \times m$ pixel neighborhood, as long as the occluding object is still contained within that neighborhood, or likewise by increasing n, the number of frames in the matched path, as long as the occluding object is recorded in those additional frames. Theoretically, the parameter λ could be increased by detecting more photons in each sun background pixel, for example, by simultaneously increasing exposure time and detector well depth.

V. Testing the Theoretical Resolution Limit

For the transit events in Figs. 2a and 2b, a detection statistic was measured from the data by normalizing the matched path summation (containing or matched to the Terra occluding shadow) with the measured mean and standard deviation of all the simultaneous parallel path summations. This measured detection statistic was compared with the predicted detection statistic from Eq. (13) over varying path parameters n and m. To predict Eq. (13), λ was calculated to be 13,600 photons per pixel by scaling the mean signal over all $\{i, j, k\}$ pixel locations containing the sun background during exposure times less than 1 ms.

It was found in plotting the measured (dashed) and predicted (solid) z scores in Figs. 4a and 4b that the measured z-score detection statistic only fit half the value of the predicted detection statistic from Eq. (13). The reason may be attributable to experimental error. Part of this error must be due to filter mismatch, which, though generally ignored in the derivation, may cause an unavoidable loss in the experimental detection measurements. Also contributing to the

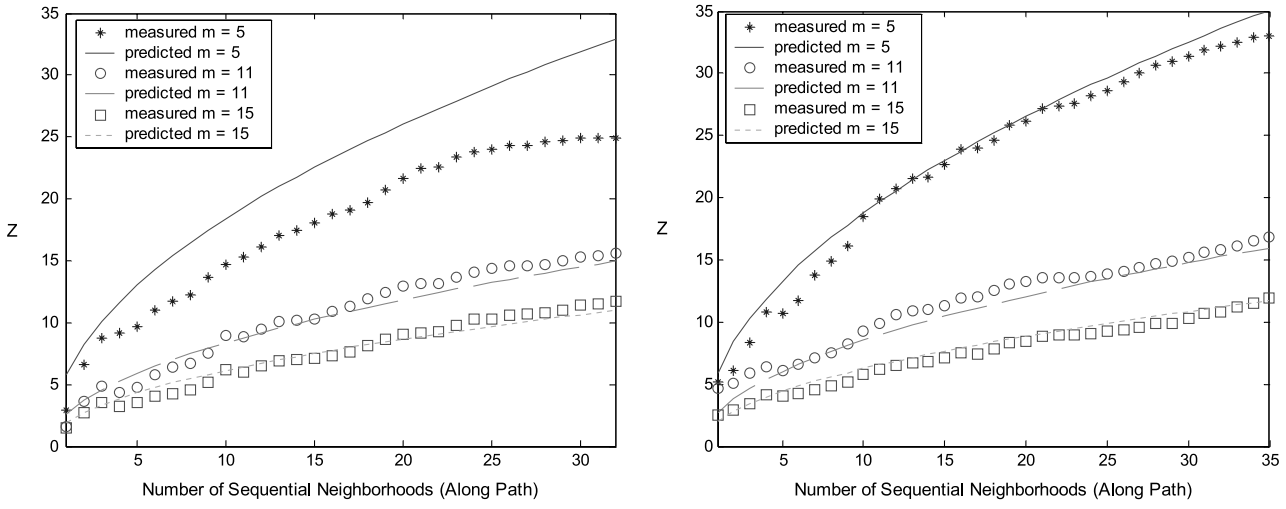

Fig. 4 Measured Terra detection statistics compared to half of Eq. (13) for a) 2007, and b) 2008.

observed error, the measured standard deviation of the data σ_d was generally found to be larger than the predicted from Eq. (12). This is likely due to an increasing departure of real data from the uniform sun approximation, especially for larger $m \times m$ neighborhoods. The causes of these deviations from the predicted model include the motion of the sun's structure in the image from jitter, atmospheric particles, and the sun's intensity variation due to atmospheric scintillation. Another effect of these accumulated deviations on the distribution of real path summations is that the false alarm rate is greater than the expected standard normal false alarm rate.

Note the measured $m = 5$ curve of Fig. 3a is less than that in Fig. 3b. This should be expected because of additional blurring caused by the extra glass window in 2007. Then, the $m = 5$ neighborhood integrated a smaller total occluding area in the 2007 event than in the 2008 event. But as seen in Figs. 3a and 3b, larger neighborhoods compensated for this blurring. Further experimental research is required to show if and under what circumstances the photometric limits of detection outlined in Eq. (13) may be achievable for experimental systems.

VI. General Limitations and Capabilities of an Occluded-Sunlight Detection System

Experimental limitations in the described system prevented the detection of any other satellites or orbital debris. Theoretically, the experimental system should be able to detect occlusions as small as 0.25 pixel areas over a matched path, but no objects of this size were imaged. Smaller objects (uncontrolled rocket bodies, less than 0.15 pixel areas) were imaged, but they could not be detected convincingly, partly because the experimental data had an inflated false alarm rate.

Like typical nighttime detection, these sun-occlusion observations are limited by weather and atmosphere constraints. The nature of these observations also imposes additional limitations over nighttime observations. One limitation is the telescope pointing and field of view is restricted to the area of the sky within the disk of the sun. Another limitation of these observations is that any atmospheric particles that pass between the telescope and sun will also cause occluding shadows, and these can cause detection false alarms, different than the typical nighttime observations, which exclude the detection of atmospheric particles when these particles are in the Earth's shadow, and so not illuminated by sunlight.

Still, there may be several practical reasons to use this form of sun-occlusion observation for the detection of satellites and orbital debris. These observations should have the ability to characterize nonreflective debris which may not be detectable in nighttime observations. Also, these observations could provide a daytime role for telescopes and additional observations of satellites and debris for catalog maintenance tasks. The ability to discern projected areas may be useful for larger objects or to characterize the changing areas of tumbling orbital debris.

Designing a ground-based optical system effective in detecting smaller debris is possible by engineering Eq. (13). By using more pixels and increasing resolution to the diffraction limits of the atmosphere (e.g., 2.7×10^{-4} deg per pixel), the total occluding area of an object shadow can be increased. Using a narrowband of wavelengths instead of white light may be helpful in reducing spatial blurring and reducing the spatial neighborhood size m. A faster sampling rate can improve resolution by increasing the length of the path n. Also, maximizing the photon count per pixel λ can improve resolution, as long as the number of digital levels in the sensor does not oversample the photon count. Then, the gain in the detection statistic from increased sampling rate and increased photon detection is $\sqrt{n}$ and $\sqrt{\lambda}$, but, for practical systems, the gain may be bounded by atmospheric and system noise. If such a system could reliably detect a 0.01 pixel area occlusion, this would correspond to detecting a 2.7×10^{-6} deg-diam object at the atmospheric limit of 2.7×10^{-4} deg per pixel.

VII. Conclusions

Novel aspects of these observations of occluded sunlight in sun transit images have been introduced and explored here. The general model proposed should be useful in making approximations about the achievable resolutions of theoretical sunlight-occlusion detection systems. However, for real systems, the limitations affecting these observations have not yet been precisely modeled. Further research is necessary to more fully model the experimental limitations of the proposed detection method in resolving smaller size orbital debris.

Acknowledgments

The experimental equipment used in this research was funded through the University of Colorado by a Beverly Sears Grant and a Sigma-Xi Grant-in-Aid of Research.

References

[1] Pohlig, S. C., "Spatial Temporal Detection of Electro-Optic Moving Targets," *IEEE Transactions on Aerospace and Electronic Systems*, Vol. 31, No. 2, April 1995, pp. 608–616. doi:10.1109/7.381909

[2] Sanders-Reed, J. N., "Maximum Likelihood Detection of Unresolved Moving Targets," *IEEE Transactions on Aerospace and Electronic Systems*, Vol. 34, No. 3, July 1998, pp. 844–859. doi:10.1109/7.705892

[3] Moutou, C., and Pont, F., "Detection and Characterization of Extrasolar Planets: The Transit Method," *Planetary Formation and Exoplanets*, Strausbourg Astronaumical Observatory and The French Society of Astronomy and Astrophysics, Strausbourg, France, 2006, pp. 55–79.

[4] Kurkland, R., Schurig, H., Rosenfeld, M., Herriage, M., Gaddy, E., Keys, D., Faust, C., Andiario, W., Kurtz, M., and Moyer, E., "Terra Flexible Blanket Solar Array Development, On-Orbit Performance and Future Applications," *Photovoltaic Specialists Conference*, Inst. of Electrical and Electronics Engineers, New York, 2000, pp. 1061–1066.

[5] Davis, J. C., *Statistics and Data Analysis in Geology*, Wiley, New York, 1986, pp. 52–53.

[6] Delouille, V., Chainais, P., and Hochedez, J.F., "Spatial and Temporal Noise in Solar EUV Observations," *Solar Physics*, Vol. 248, No. 2, April 2008, pp. 441–455. doi:10.1007/s11207-008-9131-x

D. Spencer
Associate Editor